

## Research Article

# Synthesis, Spectral Characterization, and Thermal and Cytotoxicity Studies of Cr(III), Ru(III), Mn(II), Co(II), Ni(II), Cu(II), and Zn(II) Complexes of Schiff Base Derived from 5-Hydroxymethylfuran-2-carbaldehyde

Amani S. Alturiqi,<sup>1</sup> Abdel-Nasser M. A. Alaghaz ,<sup>2,3</sup>  
Reda A. Ammar,<sup>4,5</sup> and Mohamed E. Zayed<sup>6</sup>

<sup>1</sup>Department of Chemistry, College of Science, Princess Nourah Bint Abdulrahman University, Riyadh, Saudi Arabia

<sup>2</sup>Department of Chemistry, Faculty of Science, Jazan University, Jazan, Saudi Arabia

<sup>3</sup>Department of Chemistry, Faculty of Science (Boys), Al-Azhar University, Cairo, Egypt

<sup>4</sup>Department of Chemistry, College of Sciences Al Imam Mohammad Ibn Saud Islamic University (IMSIU), Riyadh 11623, Saudi Arabia

<sup>5</sup>Department of Chemistry, Faculty of Science (Girls), Al-Azhar University, Cairo, Egypt

<sup>6</sup>Department of Botany and Microbiology, Faculty of Science, King Saud University, Riyadh 11541, Saudi Arabia

Correspondence should be addressed to Abdel-Nasser M. A. Alaghaz; aalaghaz@hotmail.com

Received 24 December 2017; Revised 18 February 2018; Accepted 8 March 2018; Published 9 May 2018

Academic Editor: Josefina Pons

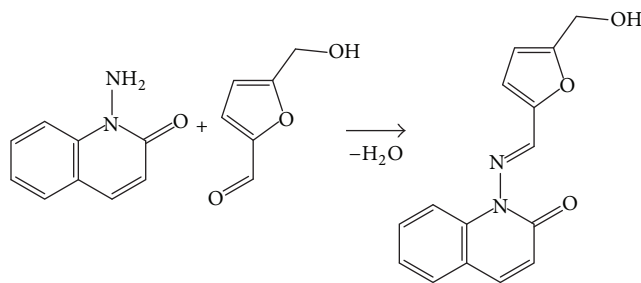
Copyright © 2018 Amani S. Alturiqi et al. This is an open access article distributed under the Creative Commons Attribution License, which permits unrestricted use, distribution, and reproduction in any medium, provided the original work is properly cited.

Coordination compounds of Cr(III), Ru(III), Mn(II), Co(II), Ni(II), Cu(II), and Zn(II) ions were synthesized from the furan ligand [5-hydroxymethylfuran-2-yl-methyleneaminoquinolin-2-one] (H-MFMAQ) derived from the condensation of 5-hydroxymethylfuran-2-carbaldehyde and 1-aminoquinolin-2(1H)-one. Elemental analytical data, IR, NMR (<sup>1</sup>H, <sup>13</sup>C, and <sup>15</sup>N), EPR, XRD, SEM, TEM, EDX, TGA, mass, molar conductance, magnetic moment, and UV-Visible spectra techniques were used to confirm the structure of the synthesized chelates. According to the data obtained, the composition of the 1:1 metal ions : furan Schiff base ligand was found to be [M(MFMAQ)Cl<sub>2</sub>] (M = Cr(III) and Ru(III)) and [M(MFMAQ)Cl(H<sub>2</sub>O)]·nH<sub>2</sub>O in which (M = Mn(II); n = 1, Co(II); n = 0, Ni(II); n = 2, Cu(II); n = 0 and Zn(II); n = 2.5). The measurements of magnetic susceptibility, ligand field parameter, and reflectance spectra suggested an octahedral geometry for the complexes. Central metals ions and furan Schiff base coordinated via O3 and N donor sites which was observed from IR spectra. The cytotoxic activities of all inspected compounds were evaluated towards *human breast (MCF-7) and lung cancer (A549) cell lines*.

## 1. Introduction

Transition metal complexes derived from the Schiff base ligands with biological potency have been broadly studied. Schiff bases appear to be an important intermediate in a number of enzymatic reactions including interaction of an enzyme with an amino or a carbonyl group of the substrate. The biochemical process which involves the condensation of a primary amine in an enzyme may be one of the most important catalytic mechanisms kinds [1]. Transition metal complexes with different oxidation states have a strong role

in bioinorganic chemistry and may give the models basis for active sites of biological systems [2–4]. For a long time, it had been identified as a serious cofactor in biological compounds, either as a compositional template in protein folding or as a Lewis acid catalyst which can readily adopt the coordination numbers 4, 5, or 6 [5, 6]. Coordination chemistry of cobalt complexes was a substantial importance as a result of the toxic environmental effect of cobalt. The cobalt mobilization and immobilization in the climate, organisms, and approximately technical systems (such as in ligand exchange chromatography) have been presented manifestly to depend



SCHEME 1: Synthetic route of ligand H-MFMAQ.

on the complexation of the metal center by chelating nitrogen donor ligands [7]. The size and shape of the nanomaterials are considered the key factors for shaping their characteristics such as electrical, optical, magnetic, antimicrobial, and catalytic potency. Metal and metal oxide nanoparticles have found a wide range of uses, including heterogeneous catalysts, environmental remediation, electronics, chemical sensing devices, medicinal fields, separations, thin films, inks, disinfection, and antimicrobial activity [8]. These different applications altered with morphology and size of those metal and metal oxide nanoparticles [9]. Detection of metal ions of biological importance has attracted much attention. Like  $\text{Zn}^{2+}$  ion fluorescent probes or sensors have achieved special interest.  $\text{Zn}^{2+}$  is an essential trace element and the second (after  $\text{Cu}^{2+}$ ) most abundant metal ion in humans [10, 11]. In our present work, novel  $[\text{M}(\text{MFMAQ})\text{Cl}_2]$  ( $\text{M} = \text{Cr}(\text{III})$  and  $\text{Ru}(\text{III})$ ) and  $[\text{M}(\text{MFMAQ})\text{Cl}(\text{H}_2\text{O})] \cdot n\text{H}_2\text{O}$  ( $\text{M} = \text{Mn}(\text{II}); n = 1, \text{Co}(\text{II}); n = 0, \text{Ni}(\text{II}); n = 2, \text{Cu}(\text{II}); n = 0$  and  $\text{Zn}(\text{II}); n = 2.5$ ) complexes were discussed using different studding techniques such as elemental analyses, molar conductance, magnetic moment, and UV-Vis., IR, NMR ( $^1\text{H}$ ,  $^{13}\text{C}$  and  $^{15}\text{N}$ ), mass, EPR, XRD, SEM, TEM, EDX, and TGA behavior. Also, the ligand (H-MFMAQ) and its complexes show remarkable cytotoxicity against *human breast* (MCF-7) and *lung cancer* (A549) cell lines.

## 2. Experimental

**2.1. Materials and Methods.** All the metal salts were gained from E-Merck and used without further purification. Solvents MeOH, EtOH, DMF, DMSO, and agar were procured from Hi-media chemicals. However, the solvents were purified by the standard procedures. Elemental analyses were performed on a Perkin Elmer 2400 CH/N Analyzer. Metal contents were determined complexometrically by standard EDTA titration and the Cl was tested gravimetrically using  $\text{AgNO}_3$ . Electronic spectra of the complexes were recorded on a Shimadzu Model 1601 UV-Visible Spectrophotometer. Infrared spectroscopy measurements were performed on an Agilent Cary 630 FTIR spectrometer, using the Attenuated Total Reflectance (ATR) method, with a diamond cell. Spectra were recorded from  $4000$  to  $400\text{ cm}^{-1}$ , with 64 scans and resolution of  $4\text{ cm}^{-1}$ . The  $^1\text{H}$  and  $\{^{15}\text{N}, ^1\text{H}\}$  correlation NMR spectra of samples were recorded in a Bruker Avance III 500 MHz (11.7 T) spectrometer. The  $^1\text{H}$  NMR spectrum of samples was recorded in a Bruker Avance III 600 MHz (14 T)

spectrometer. The  $\{^{15}\text{N}, ^1\text{H}\}$  NMR correlation spectrum of samples was recorded in a Bruker Avance III 400 MHz (9.4 T) spectrometer. The samples were analyzed in a  $d_6$ -DMSO solution and the chemical shifts were given relative to tetramethylsilane (TMS). The  $^{13}\text{C}$  and  $^{15}\text{N}$  solid state NMR (SSNMR) spectra were recorded in a Bruker 300 MHz spectrometer, using the combination of cross-polarization, proton decoupling, and magic angle spinning (CP/MAS) at 10 kHz. Electrospray ionization mass spectrometry (ESI-MS) measurements were carried out using a Waters Quattro Micro API. Samples were evaluated in the positive mode. Ligand was analyzed in a 1:1 methanol: water solution with addition of 0.10% (v/v) formic acid;  $\text{Cu}(\text{II})$  complex was analyzed in a 1:1 acetonitrile: water with 0.10% (v/v) formic acid;  $\text{Co}(\text{II})$  and  $\text{Ru}(\text{III})$  complexes were dissolved in a minimum amount of DMF and further dissolved in a 1:1 methanol: water solution with addition of 0.10% (v/v) formic acid immediately before the experiments. Each solution was directly infused into the instrument's ESI source and analyzed in the positive mode, with capillary potential of 3.00 kV, trap potential of 2 kV, source temperature of  $150^\circ\text{C}$ , and nitrogen gas for desolvation. Room temperature magnetic susceptibility measurements were carried out on a modified Gouy-type magnetic balance, Hertz SG8-5HJ. The room temperature molar conductivity of the complexes in MeOH, EtOH, and DMSO solutions ( $0.001\text{ mol}\cdot\text{L}^{-1}$ ) was measured using a deep vision 601 model digital conductometer. The X-band EPR spectrum was performed at LNT (77 K) using TCNE as the g-marker. Powder X-ray diffraction patterns were recorded with a X'Pert PRO Diffractometer using  $\text{CuK}\alpha_1$  radiation ( $\lambda = 1.54060\text{ \AA}$ ) with operating voltage 40 kV and a current of 30 mA. Thermal studies were carried out using Q 600SDT and Q 20 DSC thermal analyzer. SEM images were recorded in a Hitachi SEM analyzer and transmission electron microscopy (TEM) images were taken by Zeiss-EM10C-100 KV. Energy Dispersive X-Ray Analysis (EDX) (EDAX Falcon System) was conducted to analyze the presence of elements in the specimens that have been sputtered with carbon black. The cytotoxic activity of the inspected free ligand and complexes (1-7) was studied towards *human breast* (MCF-7) and *lung cancer* (A549) cell lines at the Regional Center for Microbiology and Biotechnology, Al-Azhar University as well as the other biological activities.

**2.2. Synthesis of Schiff Base Ligand (H-MFMAQ).** New Schiff base ligand (H-MFMAQ) (Scheme 1) was prepared when

TABLE 1: Analytical and physical data of the ligand H-MFMAQ and complexes 1–7.

Number	Compound (formula wt.) [M.Wt.]	Color	M.P. °C	Yield%	Elemental analysis calc. (found)				
					C%	H%	N%	Cl%	M%
1	H-MFMAQ (C <sub>15</sub> H <sub>12</sub> N <sub>2</sub> O <sub>3</sub> ) [268.3]	Pale yellow	146	91	67.16 (67.13)	4.51 (4.49)	10.44 (10.42)	--	--
	[Cr(MFMAQ)Cl <sub>2</sub> ] (C <sub>15</sub> H <sub>11</sub> Cl <sub>2</sub> CrN <sub>2</sub> O <sub>3</sub> ) [390.2]	Dark brown	211	78	46.18 (46.12)	2.84 (2.82)	7.18 (7.14)	18.17 (18.11)	13.33 (13.32)
2	[Ru(MFMAQ)Cl <sub>2</sub> ] (C <sub>15</sub> H <sub>12</sub> Cl <sub>2</sub> N <sub>2</sub> O <sub>3</sub> Ru) [439.2]	Black	219	83	41.02 (40.97)	2.52 (2.50)	6.38 (6.34)	16.14 (16.10)	23.01 (23.00)
3	[Mn(MFMAQ)Cl(H <sub>2</sub> O)]·H <sub>2</sub> O (C <sub>15</sub> H <sub>15</sub> ClMnN <sub>2</sub> O <sub>5</sub> ) [393.7]	Wine red	224	82	45.76 (45.73)	3.84 (3.83)	7.12 (7.11)	9.00 (8.98)	13.95 (13.91)
4	[Co(MFMAQ)Cl(H <sub>2</sub> O)] (C <sub>15</sub> H <sub>13</sub> ClCoN <sub>2</sub> O <sub>4</sub> ) [379.7]	Olive	218	84	47.45 (47.42)	3.45 (3.43)	7.38 (7.33)	9.34 (9.32)	15.52 (15.50)
5	[Ni(MFMAQ)Cl(H <sub>2</sub> O)]2H <sub>2</sub> O (C <sub>15</sub> H <sub>17</sub> ClN <sub>2</sub> NiO <sub>6</sub> ) [415.5]	Brown	226	77	43.37 (43.34)	4.12 (4.10)	6.74 (6.72)	8.53 (8.51)	14.13 (14.10)
6	[Cu(MFMAQ)Cl(H <sub>2</sub> O)] (C <sub>15</sub> H <sub>13</sub> ClCuN <sub>2</sub> O <sub>4</sub> ) [384.3]	Grass green	233	86	46.88 (46.83)	3.41 (3.38)	7.29 (7.23)	9.23 (9.20)	16.54 (16.51)
7	[Zn(MFMAQ)Cl(H <sub>2</sub> O)]·2.5H <sub>2</sub> O (C <sub>15</sub> H <sub>18</sub> ClN <sub>2</sub> O <sub>6.5</sub> Zn) [431.1]	Yellow	208	73	41.79 (41.72)	4.21 (4.18)	6.50 (6.48)	8.22 (8.19)	15.16 (15.12)

5-hydroxymethylfuran-2-carbaldehyde (1.24 g, 11.23 mmol) was added to 1-aminoquinolin-2(1H)-one (1.79 g, 11.23 mmol), both dissolved in absolute ethanol (50 ml). Mixture was heated under reflux for 3 h to be a pale-yellow precipitate and was formed upon cooling the solution to room temperature. The product was filtered off and washed with few amounts of ethanol then diethyl ether, air-dried, and recrystallized from ethanol. The yield was 2.77 g (91%). The physical properties and analytical data of the furan Schiff base ligand and its metal complexes are scheduled in Table 1.

**2.3. Synthesis of Schiff Base Metal(II/III) Complexes.** A mixture of furan Schiff base ligand H-MFMAQ (6.76 mmol; 1.81 g) dissolved in an ethanol (20 ml) and chloride salt of Cr (III), Ru(III), Mn(II), Co(II), Ni(II), Cu(II), or Zn (II) (6.76 mmol) dissolved in the same solvent (20 ml) was heated for two hours under reflux on a water bath. The formed precipitate was filtered off, washed with ethanol and diethylether, and finally dried to give [Cr(MFMAQ)Cl<sub>2</sub>] (1), [Ru(MFMAQ)Cl<sub>2</sub>] (2), [Mn(MFMAQ)Cl(H<sub>2</sub>O)]·H<sub>2</sub>O (3), [Co(MFMAQ)Cl(H<sub>2</sub>O)] (4), [Ni(MFMAQ)Cl(H<sub>2</sub>O)]·2H<sub>2</sub>O (5), [Cu(MFMAQ)Cl(H<sub>2</sub>O)] (6), and [Zn(MFMAQ)Cl(H<sub>2</sub>O)]·2.5H<sub>2</sub>O (7) complexes.

### 3. Results and Discussions

**3.1. Ligand (H-MFMAQ).** H-MFMAQ percentage of purity was 99.97%; it has been measured by HPLC. Mass spectrum of the furan Schiff base ligand (H-MFMAQ) (Figure 1(a)) has final peak at 268 amu corresponding to the furan Schiff base ligand moiety [C<sub>15</sub>H<sub>12</sub>N<sub>2</sub>O<sub>3</sub>] (atomic mass 268 amu) (Scheme 2). Other peaks like 52, 82, 148, 152, 208, and 227 amu were suggested according to diverse fragments. From this study, it was found that the intensity of the peaks gave information on the stability of fragmentation. The electronic spectrum of furan Schiff base ligand (H-MFMAQ)

in ethanol exhibited five absorption bands (Figure 2(a)) at 233–338 nm regions which is due to  $\pi \rightarrow \pi^*$  and  $n \rightarrow \pi^*$  transitions utilizing molecular orbital of the quinoline and furan rings, C=N and C=O groups. Nevertheless, the IR spectrum of furan Schiff base ligand (H-MFMAQ) (Figure 3(a)) does not show any band at 1700 cm<sup>-1</sup>, 3380 cm<sup>-1</sup>, and 3250 cm<sup>-1</sup> corresponding to the carbonyl groups and free primary amino groups; this confirms the complete condensation between keto and amino groups. The band at 1637 cm<sup>-1</sup> is corresponding to  $\nu$  (CH=N) stretching vibration. The IR spectrum of furan Schiff base ligand (H-MFMAQ) displays a broad band at 3483 cm<sup>-1</sup>, which can be assigned to  $\nu$ (OH) group. The <sup>1</sup>H-NMR spectra of the furan Schiff base ligand (H-MFMAQ) (Figure 4(a)) exhibit signals due to aromatic protons as multiplet at  $\delta$  6.80–7.23 (8H) and a broad signal at  $\delta$  (11.35) ppm is assigned for O–H proton, which disappeared with addition of D<sub>2</sub>O due to the proton exchange. In <sup>13</sup>C NMR of ligand (H-MFMAQ) (Figure 5(a)) ( $\underline{\text{C}}=\text{O}$ ) carbonyl carbon showed signal at 166.47 ppm, ( $\underline{\text{C}}=\text{N}$ -) azomethine carbon at 162.12 ppm, ( $\underline{\text{C}}-\text{O}$ ) phenolic group carbon at 158.27 ppm, and ( $\underline{\text{C}}-\text{O}$ ) furan ring at 170.12. The spectrum <sup>15</sup>N-NMR of the ligand (H-MFMAQ) (Figure 6(a)) shows two signals centered 244.3 and 163.3 ppm, which were assigned to N12 (azomethine) and N1 (quinoline), respectively.

**3.2. Complexes.** The empirical formulae of complexes showing number of water molecules are presented in Table 1. All synthesized solid complexes are stable in air. They are practically insoluble in water, but on the contrary quite soluble in polar organic solvents (e.g., EtOH, MeOH, DMF, and DMSO). The structures of the complexes could not be determined because single crystals were not obtained. The molar conductivity data (Table 2) clearly indicate that all complexes in MeOH and DMSO as well as Cr(III), Ru(III), Mn(II), Co(II), Ni(II), Cu(II), and Zn(II) complexes in MeOH,

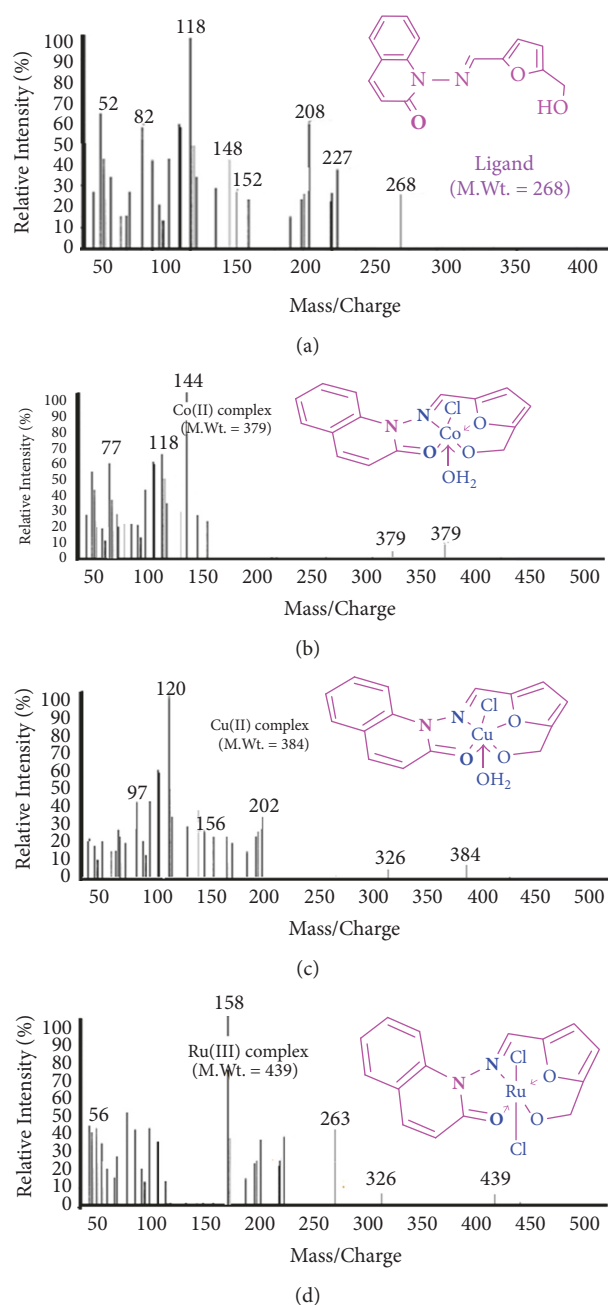


FIGURE 1: Mass spectrum of (a) ligand, (b) Co(II) complex, (c) Cu(II) complex, and (d) Ru(III) complex.

DMF, and DMSO are in the range  $7.58\text{--}15.24 \Omega^{-1} \text{cm}^2 \text{mol}^{-1}$  indicating the nonelectrolytic nature of all complexes [12]. This finding is consistent with the infrared spectral data that showed the coordinated nature of chloride anions.

**3.2.1. Mass Spectra of Complexes.** The ESI mass spectrum of the Co(II) complex  $[\text{Co}(\text{MFMAQ})\text{Cl}(\text{H}_2\text{O})]$  (Figure 1(b)) shows the parental ion peak at  $m/z = 379$  corresponding to  $(\text{CoC}_{15}\text{H}_{13}\text{ClN}_2\text{O}_4)^+$ . The other fragments of the complex give the peak with various intensities at different  $m/z$  values like at 74  $(\text{CoO})^+$ , 77  $(\text{C}_6\text{H}_5)^+$ , 144  $(\text{CoC}_4\text{H}_7\text{NO})^+$ , and 326

$(\text{CoC}_{15}\text{H}_{11}\text{N}_2\text{O}_3)^+$ . This schematic mass spectral fragmentation pattern of ligand is consistent with its structure which is depicted in Scheme 3.

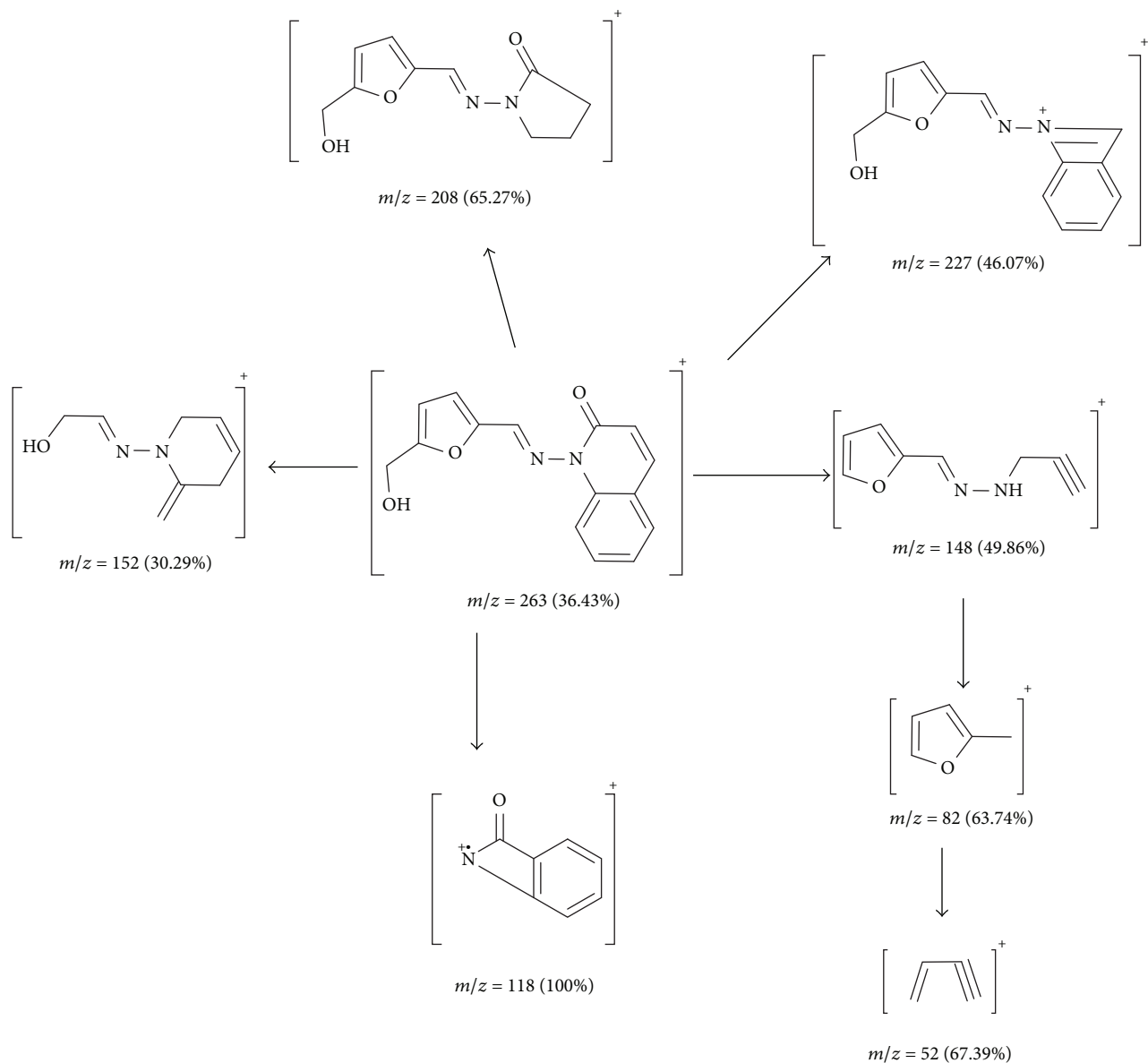
The ESI mass spectrum of the Cu(II) complex  $[\text{Cu}(\text{MFMAQ})\text{Cl}(\text{H}_2\text{O})]$  (Figure 1(c)) shows the parental ion peak at  $m/z = 384$  corresponding to  $(\text{CoC}_{15}\text{H}_{13}\text{ClN}_2\text{O}_4)^+$ . The different fragments of the complex with different  $m/z$  values are present at 97  $(\text{C}_5\text{H}_7\text{NO})^+$ , 120  $(\text{C}_7\text{H}_8\text{N}_2)^+$ , 202  $(\text{CuC}_6\text{H}_7\text{N}_2\text{O}_2)^+$ , and 326  $(\text{CuC}_{13}\text{H}_{11}\text{ClN}_2\text{O}_2)^+$ . This schematic mass spectral fragmentation pattern of ligand is consistent with its structure which is depicted in Scheme 4.

The ESI mass spectrum of the Ru(III) complex  $[\text{Ru}(\text{MFMAQ})\text{Cl}_2]$  (Figure 1(d)) shows the molecular ion peak at  $m/z = 439$  corresponding to  $(\text{RuC}_{15}\text{H}_{11}\text{Cl}_2\text{N}_2\text{O}_3)^+$ . The other fragments of the complex show the peaks at different  $m/z$  values like at 56  $(\text{C}_4\text{H}_8)^+$ , 210  $(\text{RuC}_6\text{H}_7\text{NO})^+$ , 158  $(\text{C}_{10}\text{H}_{10}\text{N}_2)^+$ , 263  $(\text{RuC}_8\text{H}_6\text{N}_2\text{O}_2)^+$ , and 326  $(\text{RuC}_{11}\text{H}_{14}\text{N}_2\text{OCl})^+$ . This schematic mass spectral fragmentation pattern of ligand is consistent with its structure which is depicted in Scheme 5. These facts were matched to the suggested molecular formula for these complexes, that is,  $[\text{Co}(\text{MFMAQ})\text{Cl}(\text{H}_2\text{O})]$ ,  $[\text{Cu}(\text{MFMAQ})\text{Cl}(\text{H}_2\text{O})]$ , and  $[\text{Ru}(\text{MFMAQ})\text{Cl}_2]$ , where MFMAQ is the ligand. This confirms the Schiff base frame formation. Elemental analysis values were appropriate with those values calculated from the molecular formulae assigned to these complexes which are further supported by mass studies.

**3.2.2. Electronic Absorption, Magnetic Measurements, and Ligand Field Parameter.** The electronic absorption spectra of the free Schiff base ligand and its complexes (Cr(III), Ru(III), Mn(II), Co(II), Ni(II), Cu(II), and Zn(II)) were studied in Nujol mull.

Two bands were showed at  $18,995$  ( $\epsilon = 46 \text{ Lmol}^{-1} \text{cm}^{-1}$ ) and  $16,238 \text{ cm}^{-1}$  ( $\epsilon = 34 \text{ Lmol}^{-1} \text{cm}^{-1}$ ); for Cr(III) complex  $[\text{Cr}(\text{MFMAQ})\text{Cl}_2]$  electronic spectrum, those may be assigned to  ${}^4\text{A}_2\text{g}(\text{F}) \rightarrow {}^4\text{T}_1\text{g}(\text{F})$  and  ${}^4\text{A}_2\text{g}(\text{F}) \rightarrow {}^4\text{T}_2\text{g}(\text{F})$  transitions, respectively, in an octahedral geometry [13], whereas the third band, which is due to  ${}^4\text{A}_2\text{g}(\text{F}) \rightarrow {}^4\text{T}_1\text{g}(\text{P})$  transition, lies in the range of the ligand transitions that were predicted at  $34,264 \text{ cm}^{-1}$  ( $\epsilon = 132 \text{ Lmol}^{-1} \text{cm}^{-1}$ ). The ligand field parameters of the current Cr(III) complex have been calculated using Tanabe-Sugano diagrams  $B$  ( $583 \text{ cm}^{-1}$ ),  $10Dq$  ( $1742 \text{ cm}^{-1}$ ), and  $\beta$  (0.53). The effective magnetic moment of the complex is 3.92 BM, which is consistent with the spin-only value for three unpaired electrons (3.87 BM) [14].

Electronic spectrum of Mn(II) complex  $[\text{Mn}(\text{MFMAQ})\text{Cl}(\text{H}_2\text{O})] \cdot \text{H}_2\text{O}$  exhibits four weak intensity absorption bands at  $17,943$  ( $\epsilon = 30 \text{ Lmol}^{-1} \text{cm}^{-1}$ ),  $22,806$  ( $\epsilon = 36 \text{ Lmol}^{-1} \text{cm}^{-1}$ ),  $27,216$  ( $\epsilon = 64 \text{ mol}^{-1} \text{cm}^{-1}$ ), and  $37,489 \text{ cm}^{-1}$  ( $\epsilon = 138 \text{ Lmol}^{-1} \text{cm}^{-1}$ ). These bands may be assigned to the transitions:  ${}^6\text{A}_1\text{g} \rightarrow {}^4\text{T}_1\text{g}$  (4G),  ${}^6\text{A}_1\text{g} \rightarrow {}^4\text{E}_\text{g}$ ,  ${}^4\text{A}_1\text{g}$  (4G) ( $10B + 5C$ ),  ${}^6\text{A}_1\text{g} \rightarrow {}^4\text{E}_\text{g}$  (4D) ( $17B + 5C$ ), and  ${}^6\text{A}_1\text{g} \rightarrow {}^4\text{T}_1\text{g}$  (4P) ( $7B + 7C$ ), respectively. The ligand parameters  $B$  and  $C$  were calculated from the second and third electronic transitions because these electronic transitions are free from the crystal field splitting and depend on  $B$  and  $C$  parameters [13, 14]. The calculated values of the ligand field parameters are given in Table 3. Room temperature magnetic moment of the Mn(II)



SCHEME 2: Mass fragmentation pattern of furan Schiff base ligand (H-MFMAQ).

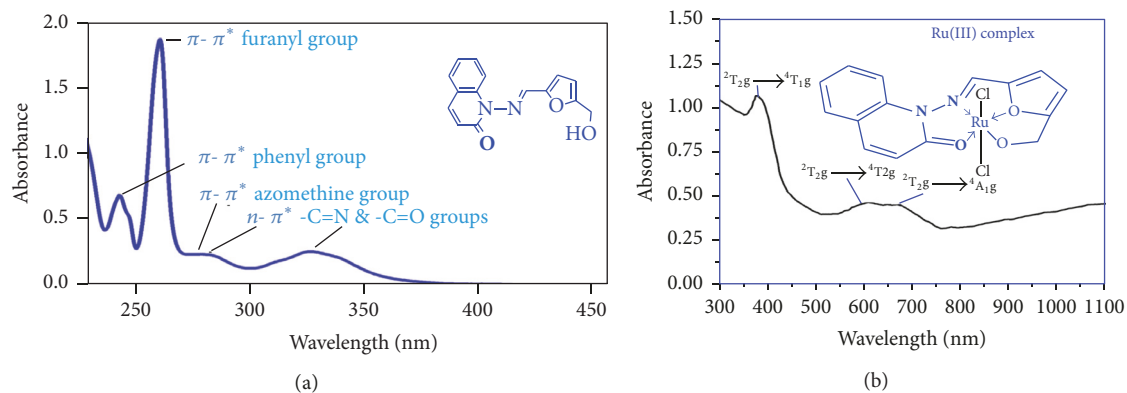


FIGURE 2: Electronic spectrum of (a) ligand and (b) Ru(III) complex.

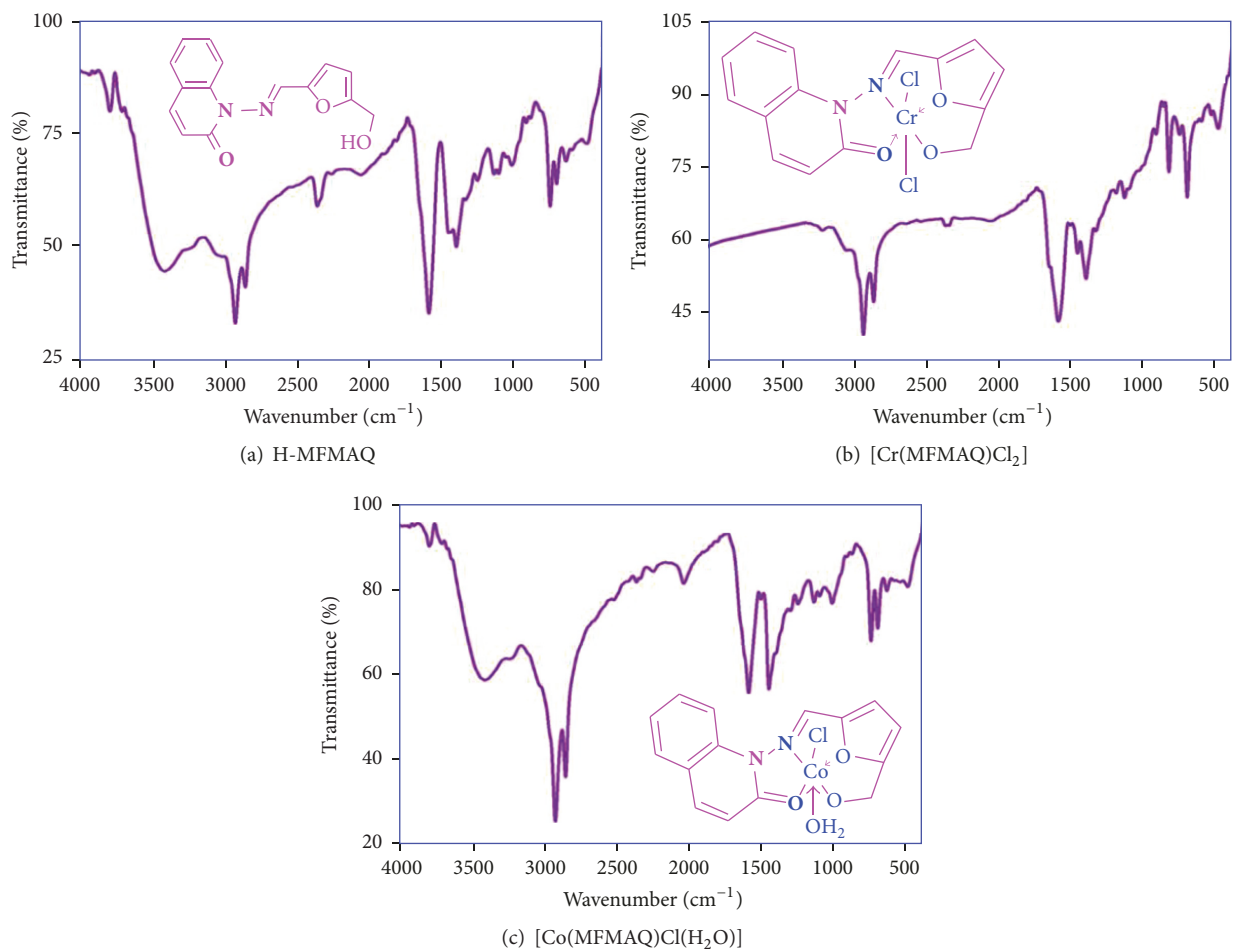


FIGURE 3: (a) IR spectrum of ligand, (b) IR spectrum of Cr(III) complex, and (c) IR spectrum of Zn(II) complex.

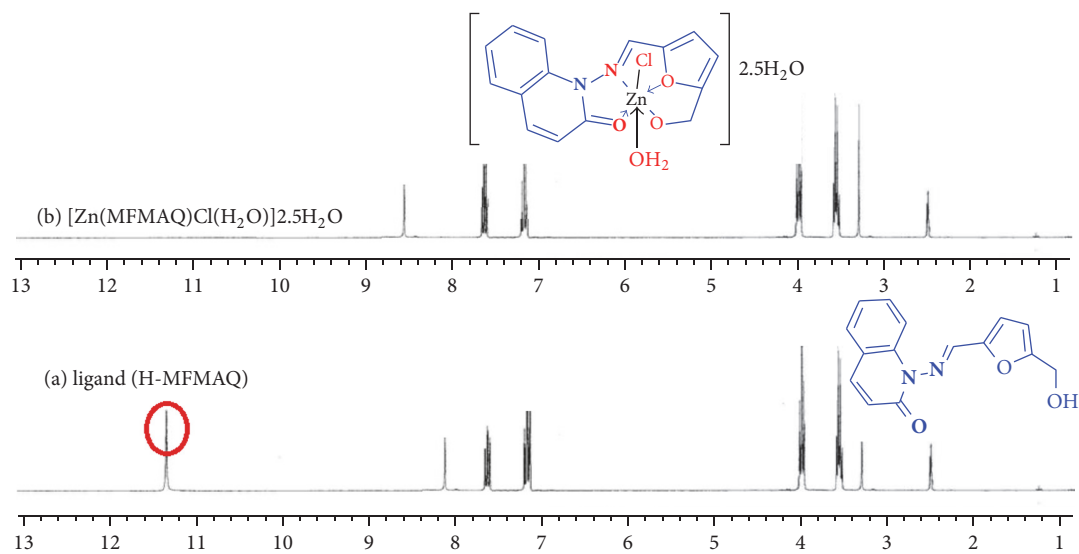
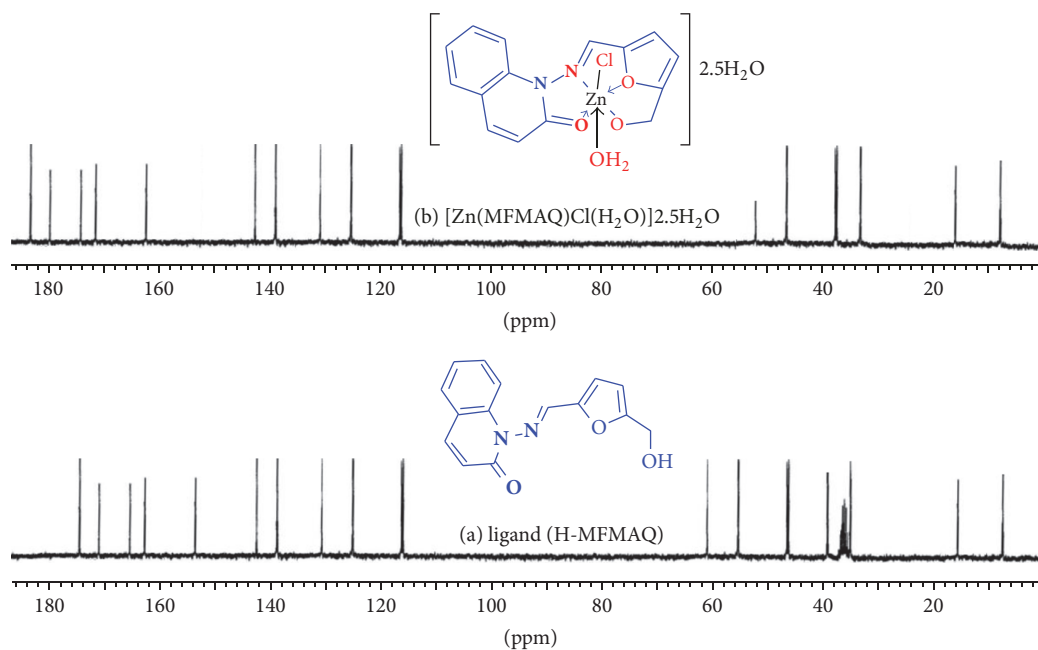
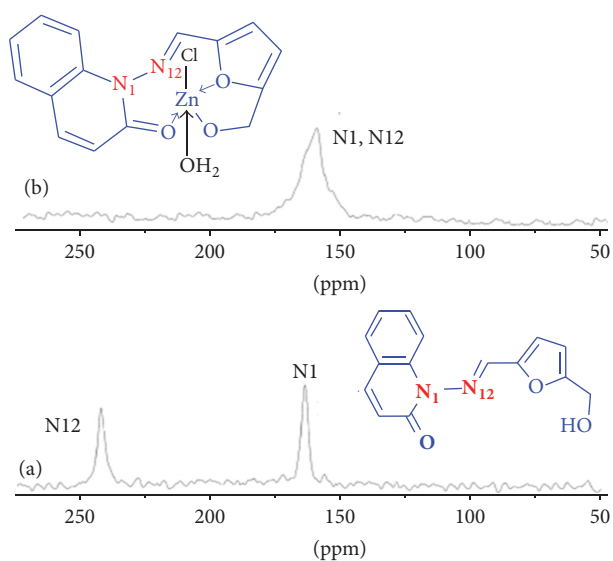
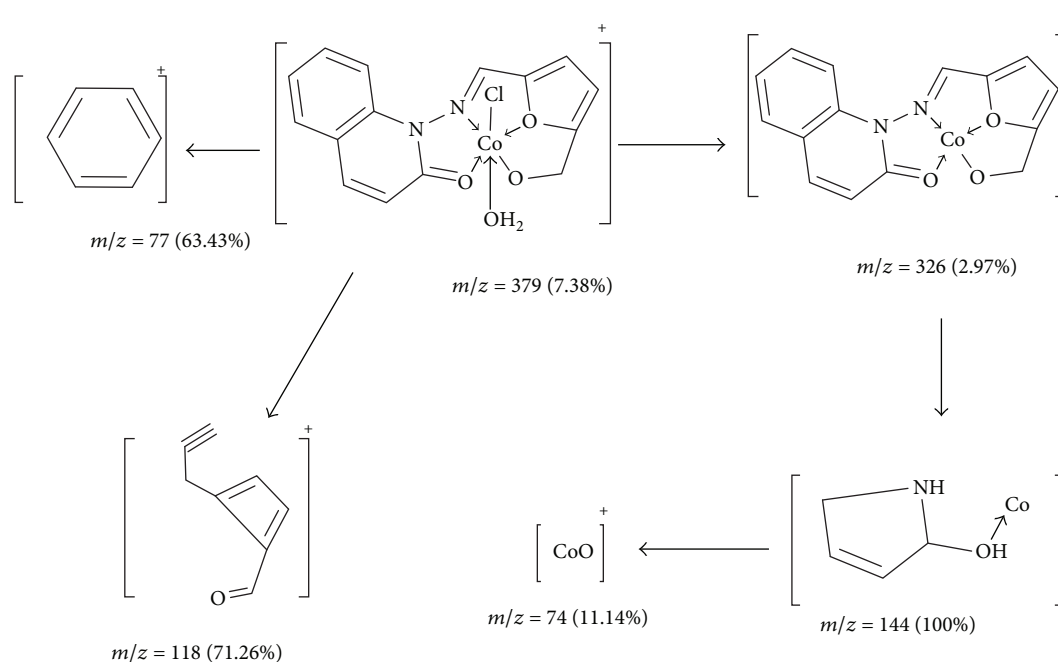


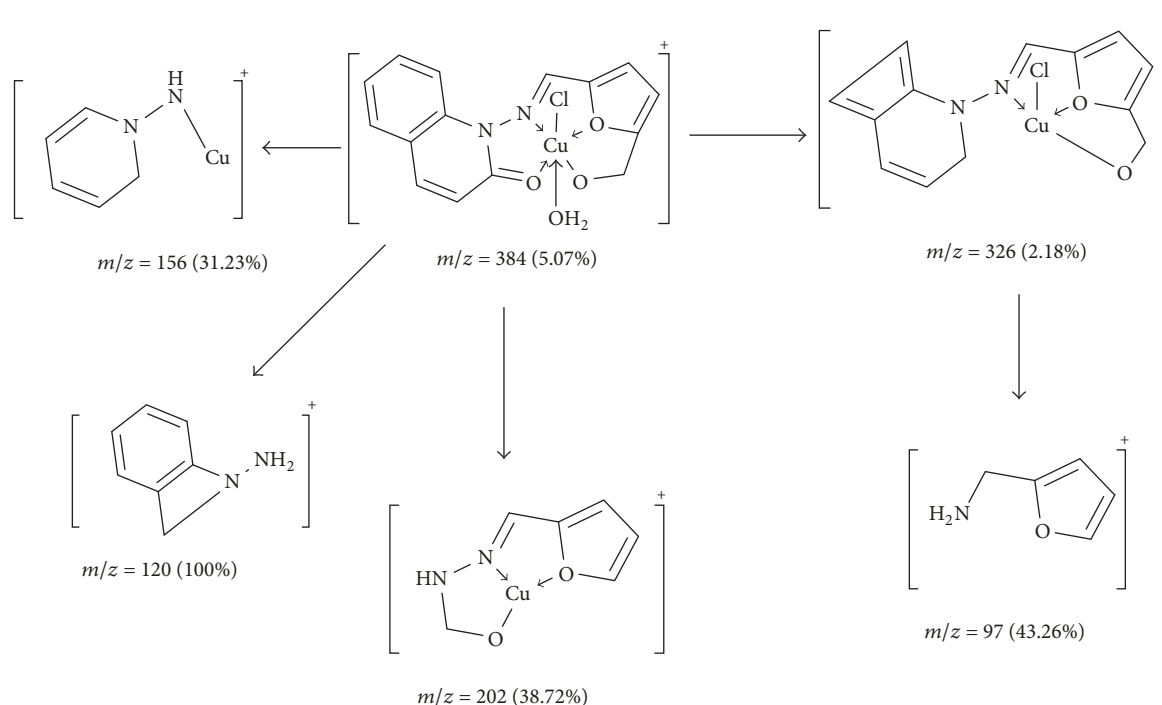
FIGURE 4:  $^1\text{H}$  NMR spectra of (a) Schiff base ligand and (b) Zn(II) complex.

FIGURE 5:  $^{13}\text{C}$  NMR spectra of (a) Schiff base ligand and (b) Zn(II) complex.FIGURE 6:  $^{15}\text{N}$  NMR spectra of (a) Schiff base ligand and (b) Zn (II) complex.TABLE 2: Molar conductivity of complexes  $\Lambda \text{ M}/\Omega^{-1} \text{ cm}^2 \text{ mol}^{-1}$  for  $0,001 \text{ mol}\cdot\text{L}^{-1}$  solutions in MeOH, DMF, and DMSO at  $25^\circ\text{C}$ .

Complex	$\Lambda_{\text{M}} [\Omega^{-1} \text{ cm}^2 \text{ mol}^{-1}]$		
	MeOH	DMF	DMSO
$[\text{Cr}(\text{MFMAQ})\text{Cl}_2]$	14.36	15.24	7.58
$[\text{Ru}(\text{MFMAQ})\text{Cl}_2]$	12.87	14.25	9.77
$[\text{Mn}(\text{MFMAQ})\text{Cl}(\text{H}_2\text{O})]\cdot\text{H}_2\text{O}$	12.42	14.85	8.56
$[\text{Co}(\text{MFMAQ})\text{Cl}(\text{H}_2\text{O})]$	11.57	13.93	8.45
$[\text{Ni}(\text{MFMAQ})\text{Cl}(\text{H}_2\text{O})]\cdot 2\text{H}_2\text{O}$	12.84	14.47	9.27
$[\text{Cu}(\text{MFMAQ})\text{Cl}(\text{H}_2\text{O})]$	10.75	13.74	7.89
$[\text{Zn}(\text{MFMAQ})\text{Cl}(\text{H}_2\text{O})]\cdot 2.5\text{H}_2\text{O}$	11.59	14.66	8.98



SCHEME 3: Mass fragmentation pattern of Co(II) complex [Co(MFMAQ)(H<sub>2</sub>O)Cl].



SCHEME 4: Mass fragmentation pattern of Cu(II) complex [Cu(MFMAQ)(H<sub>2</sub>O)Cl].

complex lies at 5.94 BM; this value is in tune with a high-spin octahedral configuration.

The electronic spectrum of cobalt (II) complex [Co(MFMAQ)Cl(H<sub>2</sub>O)] recorded in Nujol mulls exhibits three absorption peaks at 13,897 ( $\epsilon = 24 \text{ Lmol}^{-1} \text{ cm}^{-1}$ ), 15,368 ( $\epsilon = 27 \text{ Lmol}^{-1} \text{ cm}^{-1}$ ), and 25,157 ( $\epsilon = 53 \text{ Lmol}^{-1} \text{ cm}^{-1}$ )  $\text{cm}^{-1}$ , respectively. These bands can be assigned to  ${}^4T_{1g} \rightarrow {}^4T_{2g}$

(F)( $\nu_1$ ),  ${}^4T_{1g} \rightarrow {}^4A_{2g}$  (F)( $\nu_2$ ), and  ${}^4T_{1g} \rightarrow {}^4T_{1g}$  (P)( $\nu_3$ ) transitions, respectively, suggesting an octahedral geometry around Co(II) ion [13, 14]. Octahedral cobalt(II) complex, however, preserves a large orbital contribution to magnetic moment on account of  ${}^4T_{1g}$  (F) ground term and exhibits  $\mu_{\text{eff}}$  in the range 4.8–5.6 B.M [15]. The magnetic measurements reported here lie at 5.18 BM and demonstrate that the Co(II)

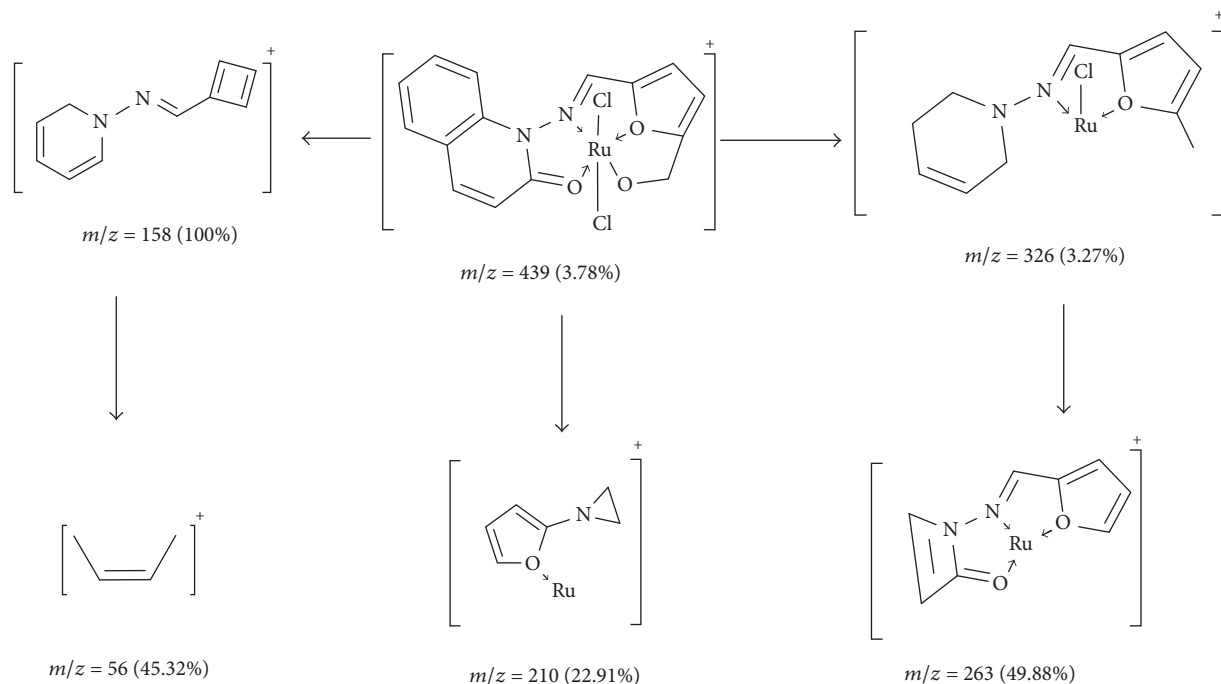
SCHEME 5: Mass fragmentation pattern of Ru(II) complex [Cu(MFMAQ)Cl<sub>2</sub>].

TABLE 3: Ligand field parameters of the complexes.

Complex	$Dq$ (cm <sup>-1</sup> )	$B$ (cm <sup>-1</sup> )	$\beta$	LFSE (kJmol <sup>-1</sup> )
[Cr(MFMAQ)Cl <sub>2</sub> ]	1674	792	0.88	208.68
[Ru(MFMAQ)Cl <sub>2</sub> ]	-	-	-	-
[Mn(MFMAQ)(H <sub>2</sub> O)Cl]·H <sub>2</sub> O	1168	808	0.73	100.47
[Co(MFMAQ)(H <sub>2</sub> O)Cl]	792	-	0.95	114.23
[Ni(MFMQ)(H <sub>2</sub> O)Cl]·2H <sub>2</sub> O	-	-	-	-
[Cu(MFMAQ)Cl(H <sub>2</sub> O)]	-	492	0.81	-
[Zn(MFMAQ)Cl(H <sub>2</sub> O)]2.5H <sub>2</sub> O	-	-	-	-

complex was paramagnetic and has a high-spin octahedral configuration with <sup>4</sup>T<sub>1g</sub>(F) ground state.

The ligand field parameters (Table 3)  $B$  (interelectronic repulsion of the d-electrons in complex),  $\beta$  (The Nephelauxetic effect), and  $10Dq$  are calculated according to the equation reported for the octahedral Co(II) complex.

$$\mu_{\text{eff}} = 4.98(1 - 4\lambda) = 10Dq,$$

$$\lambda = -178 \text{ cm}^{-1}$$

$$B = \frac{[4(\nu_3 - 15Dq)^2 - 10Dq^2]}{[60(\nu_3 - 15Dq) - 180Dq]} \quad (1)$$

$$\nu_1 = 10Dq$$

$$\beta = \frac{B(\text{complex})}{B(\text{free ion})},$$

where  $B$  (free ion) for Co(II) is 996 cm<sup>-1</sup>. The  $10Dq$ ,  $B$ , and  $\beta$  values are 7032 cm<sup>-1</sup>, 698 cm<sup>-1</sup>, and 0.68, respectively. These

results show that the interelectronic repulsion of d-electrons in a complex is less than in the free ion. The value of  $B$  in a complex is 78% of the free ion value. The  $\beta$  value is related directly to covalence.

The reduction of  $B$  is caused by complex formation by the delocalization of the d-electron cloud on the ligand, which in turn causes the covalent bond formation. The data shows the Co(II) complex has covalent character in the metal ligand “ $\sigma$ ” bond [15].

Electronic spectrum of [Ni(MFMAQ)Cl(H<sub>2</sub>O)]·2H<sub>2</sub>O complex shows bands at 15,053 ( $\epsilon = 23 \text{ Lmol}^{-1} \text{ cm}^{-1}$ ), 17,892 ( $\epsilon = 28 \text{ Lmol}^{-1} \text{ cm}^{-1}$ ), and 22,111 cm<sup>-1</sup> ( $\epsilon = 43 \text{ Lmol}^{-1} \text{ cm}^{-1}$ ). These bands may be specified to <sup>3</sup>A<sub>2g</sub>(F)→<sup>3</sup>T<sub>2g</sub>(F)( $\nu_1$ ), <sup>3</sup>A<sub>2g</sub>(F)→<sup>3</sup>T<sub>1g</sub>(F)( $\nu_2$ ), and <sup>3</sup>A<sub>2g</sub>(F)→<sup>3</sup>T<sub>1g</sub>(P)( $\nu_3$ ) transitions, respectively. It proposes octahedral geometry of [Ni(MFMAQ)Cl(H<sub>2</sub>O)]·2H<sub>2</sub>O complex [13, 14]. The magnetic moment was evaluated which gave 3.08  $\mu\text{B}$ , for [Ni(MFMAQ)Cl(H<sub>2</sub>O)]·2H<sub>2</sub>O complex which lies in the extent (2.9–3.3  $\mu\text{B}$ ) of the Ni(II) octahedral complexes [15]. The Nephelauxetic parameter  $\beta$  (Table 3) was readily

TABLE 4: IR spectral data ( $\text{cm}^{-1}$ ) of the H-MFMAQ ligand and its metal complexes.

Number	$\nu_{\text{OH}}$	$\nu_{(\text{OH})\text{water}}$	$\nu_{\text{C=O}}$	$\nu_{\text{C=N}}$	$\nu_{(\text{C-O-C})\text{furan}}$	$\nu_{\text{M-O}}$	$\nu_{\text{M-N}}$	$\nu_{\text{M-Cl}}$
H-MFMAQ	3483br	–	1712m	1637m	1618m	–	–	–
1	–	–	1693w	1621m	1600m	543m	433w	416m
2	–	–	1698m	1622m	1600w	548s	434w	412w
3	–	3320br	1695s	1622m	1605w	552m	438m	414m
4	–	3300r	1693m	1625sh	1602m	547m	434m	41 m
5	–	3320br	1697m	1624m	1605m	552m	437m	413m
6	–	3300r	1696m	1625m	1604m	549m	435m	414m
7	–	3318br	1698m	1623m	1603m	547m	438m	415m

sh: sharp, m: medium, br: broad, s: small, and w: weak.

obtained by utilizing the correlation  $\beta = B(\text{complex})/B(\text{free ion})$ , where  $B(\text{free ion})$  for Ni(II) is  $1041 \text{ cm}^{-1}$  [15]. The value of  $\beta$  lies at 0.27. These values indicated the covalent character in metal ligand “ $\sigma$ ” bond [13].

The Cu(II) complex  $[\text{Cu}(\text{MFMAQ})\text{Cl}(\text{H}_2\text{O})]$  spectrum displayed a band at  $22,137 \text{ cm}^{-1}$  ( $\epsilon = 41 \text{ Lmol}^{-1} \text{ cm}^{-1}$ ) assigned to  ${}^2\text{E}_g \rightarrow {}^2\text{T}_2g$  transition assuming octahedral geometry around the central Cu(II) ion [15]. The emulated magnetic moment of the Cu(II) complex is 1.98 BM, which assures the octahedral structure of this complex [15].

The electronic spectrum of ruthenium(III) complex  $[\text{Ru}(\text{MFMAQ})\text{Cl}_2]$  records three bands at  $15,167$  ( $\nu_1$ ) ( $\epsilon = 22 \text{ Lmol}^{-1} \text{ cm}^{-1}$ ),  $17,353$  ( $\nu_2$ ) ( $\epsilon = 27 \text{ Lmol}^{-1} \text{ cm}^{-1}$ ), and  $25,158 \text{ cm}^{-1}$  ( $\nu_3$ ) ( $\epsilon = 61 \text{ Lmol}^{-1} \text{ cm}^{-1}$ ) (Figure 2(b)). These bands may be assigned to  ${}^2\text{T}_2g \rightarrow {}^4\text{T}_1g$ ,  ${}^2\text{T}_2g \rightarrow {}^4\text{T}_2g$ , and  ${}^2\text{T}_2g \rightarrow {}^4\text{A}_1g$  transitions in order of increasing energy. The position of bands is in tune with the prediction for octahedral complexes of the metal ions [13]. The ligand field parameters  $\Delta$ ,  $B$ , and  $\beta$  have been calculated by using the relation

$$\begin{aligned} \nu_1 &= \Delta - 4B + \frac{86(B)^2}{\Delta} \\ \nu_2 &= \Delta + 12B + \frac{2(B)^2}{\Delta\sigma}. \end{aligned} \quad (2)$$

The value of  $B$  in free ion is  $638 \text{ cm}^{-1}$ . The value of  $\beta$  indicates that there is low covalency in the metal ligand  $\sigma$ -band [16]. The Ru(III) complex shows magnetic moments at room temperature 1.76 BM, which is lower than the predicted value of 2.17 BM. The lowering in  $\mu_{\text{eff}}$  values may be due to lower symmetry ligand fields, metal-metal interaction, or extensive electron delocalization [14].

The Zn(II) complex  $[\text{Zn}(\text{MFMAQ})\text{Cl}(\text{H}_2\text{O})] \cdot 2.5\text{H}_2\text{O}$  is diamagnetic as predictable and its geometry is most likely octahedral likewise Mn(II), Cu(II), Ni(II), and Co(II) complexes of H-MFMAQ ligand [15].

**3.2.3. Infrared Spectra of Complexes.** The study of infrared spectra of the furan Schiff base H-MFMAQ comparing to their metal complexes (1–7) (Table 4; Figure 3) foremost revealed that the ligand is tetradentately coordinated to the metal ions. The bands were symbolized at  $1712$  and  $1637 \text{ cm}^{-1}$  due to the carbonyl and azomethine stretching

vibration which was shifted to lower frequency by  $14$ – $19$  and  $12$ – $16 \text{ cm}^{-1}$ , suggesting oxygen carbonyl and nitrogen azomethine involvements in complexity. At  $1618 \text{ cm}^{-1}$ , the band was assigned to the furan ring  $\nu(\text{C-O-C})$  vibrations which is also shifted to lower frequency by  $13$ – $18 \text{ cm}^{-1}$ , which is suggestive to involvement of the furan ring in chelation. Also, at  $3483 \text{ cm}^{-1}$ , the band was attributed to  $\nu_{\text{OH}}$  in the ligand (H-MFMAQ) which disappeared in its metal complexes indicating deprotonation of the OH moiety during coordination [17]. The new bands at  $543$ – $552$ ,  $433$ – $438$ , and  $412$ – $416 \text{ cm}^{-1}$  were assigned to M–O (carbonyl), M–O (phenol), M–N (azomethine) and (M–Cl) in the metal complexes spectra were observed [15, 17]. The IR results showed that the metal was harmonized through one nitrogen atom (azomethine group) and three oxygen atoms (deprotonated hydroxyl group, carbonyl group, and furan ring) besides chlorine atoms.

**3.2.4. NMR Spectra Investigation.** The proton NMR spectroscopy of H-MFMAQ ligand (Figure 4(a)) and its  $[\text{Zn}(\text{MFMAQ})\text{Cl}(\text{H}_2\text{O})] \cdot 2.5\text{H}_2\text{O}$  complex (Figure 4(b)) was evident in DMSO- $d_6$  solution employing tetramethylsilane (TMS) as internal standard. OH signal was found at  $11.35 \text{ ppm}$  in the spectrum of the ligand H-MFMAQ which completely disappeared in the spectrum of the  $[\text{Zn}(\text{MFMAQ})\text{Cl}(\text{H}_2\text{O})] \cdot 2.5\text{H}_2\text{O}$  complex. This suggests the sharing of the OH group in chelation with Zn(II) through isolation of the OH proton. The azomethine proton signal was shifted to high field in the spectrum of  $[\text{Zn}(\text{MFMAQ})\text{Cl}(\text{H}_2\text{O})] \cdot 2.5\text{H}_2\text{O}$  complex. It was looked at  $8.13 \text{ ppm}$  as compared to  $8.67 \text{ ppm}$  in the Schiff’s base H-MFMAQ. This refers to the complexity of the zinc atom through nitrogen atom azomethine. However, multiple bands assigned to the aromatic protons were found at  $6.92$ – $7.97$  and  $6.98$ – $7.96 \text{ ppm}$  in the free Schiff 22 base ligand and Zn(II) complex, respectively. The signal observed at  $3.2 \text{ ppm}$  with an integration corresponding to seven protons in the case of Zn(II) complex was assigned one coordinate water molecule and half past two hydrate water molecules.

In  ${}^{13}\text{C}$  NMR of ligand (Figure 5(a)) ( $-\text{C}=\text{O}$ ) carbonyl carbon showed signal at  $166.47 \text{ ppm}$ , ( $-\text{C}=\text{N}-$ ) azomethine carbon at  $162.12 \text{ ppm}$ , ( $-\text{C}-\text{O}$ ) phenolic group carbon at  $158.27 \text{ ppm}$ , and ( $\text{C}-\text{O}$ ) furan ring at  $170.12$ . The signals due

TABLE 5: The spin-Hamiltonian parameters of Cr(III) and Cu(II) Schiff base complexes in DMSO at 300 and 77 K.

Complex	Hyperfine constant $\times 10^{-4} \text{ cm}^{-1}$					
	$A_{\parallel}$	$A_{\perp}$	$A_{\text{iso}}$	$g_{\parallel}$	$g_{\perp}$	$g_{\text{iso}}$
[Cr(MFMAQ)Cl <sub>2</sub> ]	-	-	84	-	-	1.97
[Cu(MFMAQ)Cl(H <sub>2</sub> O)]	163	47	106	2.34	2.04	2.11

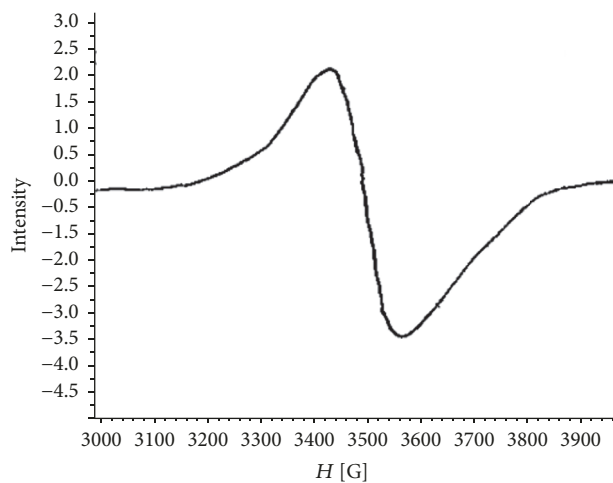
to ( $\text{--}\underline{\text{C}}=\text{N--}$ ) azomethine, ( $\text{--}\underline{\text{C}}\text{--}\text{O}$ ) phenolic, and ( $\underline{\text{C}}\text{--}\text{O}$ ) furan carbons were slightly shifted downfield in comparison to the corresponding signals of these groups in the ligand thereby confirming the complexation (Figure 5(b)) with zinc metal ion.

The <sup>15</sup>N NMR spectra of the free ligand (Figure 6(a)) and the Zn(II) complex (Figure 6(b)) were also obtained. The spectrum of the ligand shows two signals centered at 244.3 and 163.3 ppm, which were assigned to N<sub>12</sub> (azomethine) and N<sub>1</sub> (quinoline), respectively. In the spectrum of Zn(II) complex only one broad signal is observed for the nitrogen atoms at 162.7 ppm. This behavior led us to assign the broad signal in the spectra of the complexes as both N<sub>12</sub> and N<sub>1</sub> atoms. With this assignment, N<sub>12</sub> shifted 81.6 ppm downfield upon coordination to Zn(II). On the other hand, the nitrogen N<sub>1</sub> shifts only 0.6 ppm upon coordination with Zn(II). This minor shift indicates that this atom is not involved in coordination as already evidenced by other techniques.

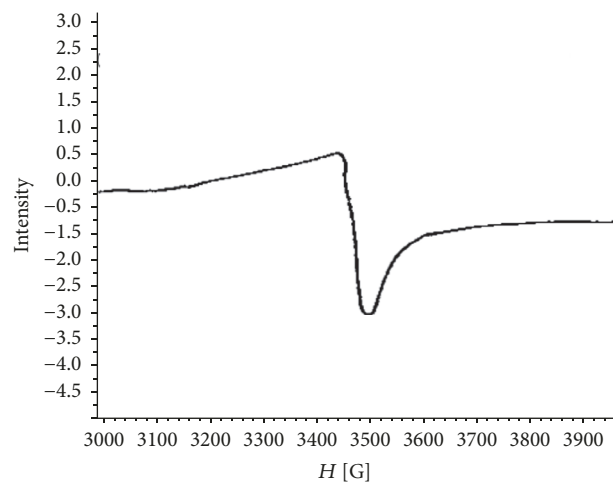
**3.2.5. ESR Spectra.** The ESR spectrum of the [Cr(MFMAQ)Cl<sub>2</sub>] complex (Table 5) has been recorded as polycrystalline sample at room temperature. No hyperfine interaction was observed in the ESR spectra of the [Cr(MFMAQ)Cl<sub>2</sub>] complex at room temperature. The  $g$ -values are calculated by using the expression,  $g = 2.0023(1 - 4\lambda/10Dq)$ , where  $\lambda$  is the spin-orbit coupling constant for the metal ion in the complex. Owen [18] gives the reduction of the spin-orbit coupling constant from the free ion value;  $90 \text{ cm}^{-1}$  for chromium(III) can be employed as a measure of metal ligand covalency (Figure 7(a)). It is possible to define a covalency parameter analogues to the Nephelauxetic parameter which is the ratio of the spin-orbit coupling constant for the complex and the free Cr(III) ions.

The solid state ESR spectrum of [Cu(MFMAQ)Cl] complex (Figure 7(b)) is displayed at room temperature. The shape of the spectrum is consistent with octahedral environment around Cu(II) ion and the higher  $g$  value for the investigated [Cu(MFMAQ)Cl] complex (Table 5), when compared to that of free electron ( $g = 2.24$ ) revealing an appreciable covalency of metal ligand bonding with  $dx^2 - y^2$  as the ground-state characteristic of octahedral stereochemistry [19]. Also, the  $g_{\parallel}/A_{\parallel}$  value 143 for the [Cu(MFMAQ)Cl] complex lies just within the range expected for octahedral complex [19]. The decrease of the  $g$ -value by 9 compared to that of the free-electron value (2.07) is an approximate measure of the ligand field strength; the stronger the furan Schiff's base ligand field, the smaller the decrease in the  $g$  value and vice versa.

**3.2.6. XRD, EDX, SEM, and TEM Morphological Studies.** In Figure 8, XRD patterns of the [Cr(MFMAQ)Cl<sub>2</sub>],



(a)



(b)

FIGURE 7: EPR spectra of (a) Cr(III) complex and (b) Cu(II) complex as polycrystalline sample.

[Co(MFMAQ)Cl(H<sub>2</sub>O)], and [Cu(MFMAQ)Cl(H<sub>2</sub>O)] complexes are depicted. The indexing procedures were performed using (CCP4, UK) CRYSFIRE program [20, 21] giving triclinic crystal system for [Cr(MFMAQ)Cl<sub>2</sub>] (Figure 8(a)) having M(9) = 7, F(6) = 8, [Co(MFMAQ)Cl(H<sub>2</sub>O)] orthorhombic crystal system (Figure 8(b)) having M(9) = 8, F(6) = 8, and tetragonal crystal system for [Cu(MFMAQ)Cl(H<sub>2</sub>O)] (Figure 8(c)) having M(6) = 14, F(6) = 6, as the superior solutions. Their cell parameters are interpreted in Table 6.

The images SEM of [Cr(MFMAQ)Cl<sub>2</sub>], [Ni(MFMAQ)Cl(H<sub>2</sub>O)]·2H<sub>2</sub>O, and [Cu(MFMAQ)Cl(H<sub>2</sub>O)]

TABLE 6: Crystallographic data for the Schiff base complexes [Cr(MFMAQ)Cl<sub>2</sub>], [Co(MFMAQ)Cl(H<sub>2</sub>O)], and [Cu(MFMAQ)Cl(H<sub>2</sub>O)].

Data	[Cr(MFMAQ)Cl <sub>2</sub> ]	[Co(MFMAQ)Cl(H <sub>2</sub> O)]	[Cu(MFMAQ)Cl(H <sub>2</sub> O)]
Empirical formula	C <sub>15</sub> H <sub>11</sub> Cl <sub>2</sub> N <sub>10</sub> O <sub>3</sub> Cr	C <sub>15</sub> H <sub>13</sub> Cl <sub>2</sub> N <sub>2</sub> O <sub>4</sub> Co	C <sub>15</sub> H <sub>13</sub> Cl <sub>2</sub> N <sub>2</sub> O <sub>4</sub> Cu
Formula weight (g/mol)	390.2	379.7	384.3
Radiation	Cu-Kα1	Cu-Kα1	Cu-Kα1
2θ range	5–60	5–60	5–60
Wavelength (Å)	1.501189	1.49997	1.52153
Crystal system	Triclinic	Orthorhombic	Tetragonal
Space group	P4/m	P4/m	P4/m
Unit cell dimensions (Å, °)			
<i>a</i> (Å)	7.986878	17.2354	7.315829
<i>b</i> (Å)	8.000534	17.2362	7.315829
<i>c</i> (°)	17.23584	16.2358	7.315829
α (°)	90	90	90
β (°)	90	90	90
γ (°)	90	90	90
Volume (Å <sup>3</sup> )	1010.47	5234.35	698.74
(Calc.) density (g/cm <sup>-3</sup> )	1.89785	1.34	1.89
Limiting indices	0 ≤ <i>h</i> ≤ 3, 0 ≤ <i>k</i> ≤ 1, 1 ≤ <i>l</i> ≤ 7	3 ≤ <i>h</i> ≤ 10, 1 ≤ <i>k</i> ≤ 6, 3 ≤ <i>l</i> ≤ 10	2 ≤ <i>h</i> ≤ 8, 1 ≤ <i>k</i> ≤ 8, 0 ≤ <i>l</i> ≤ 2
<i>Z</i>	2	6	6
<i>R<sub>f</sub></i>	0.0000901	0.000027	0.0000783
Temperature (K)	298	298	298

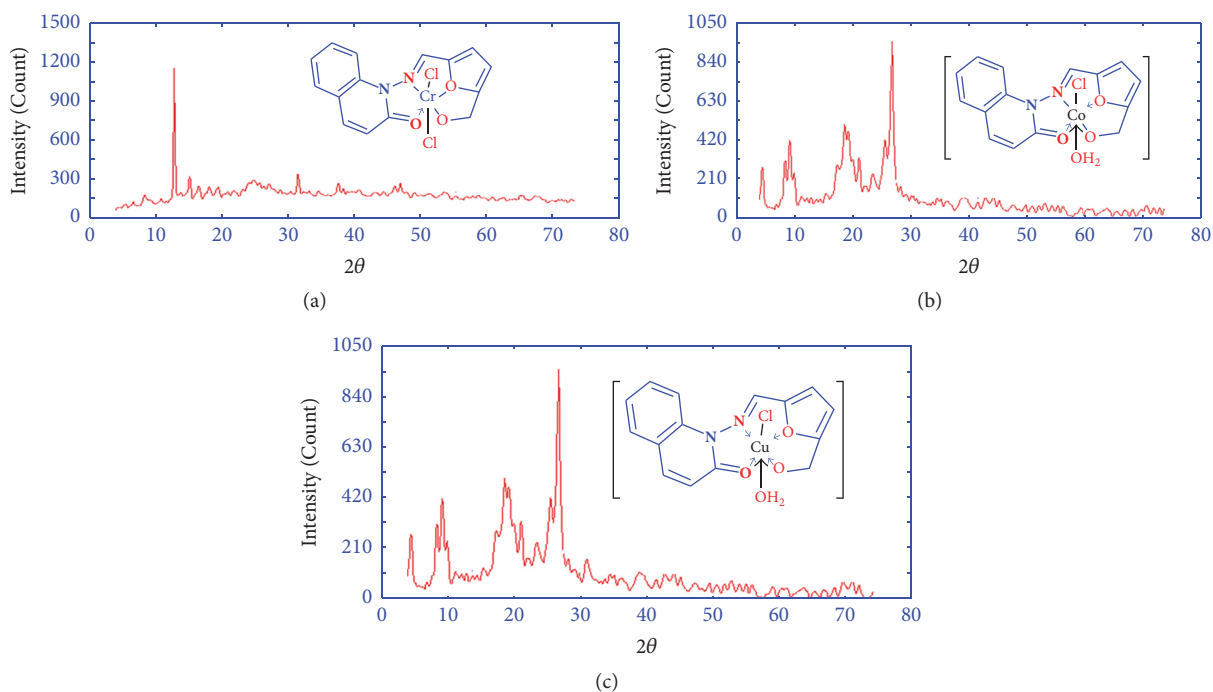


FIGURE 8: Powder XRD spectra of (a) Cr(III), (b) Co(II), and (c) Cu(II) complexes.

TABLE 7: Thermal decomposition steps of the Cr(III), Ni(II), and Cu(II) complexes in TG plots.

Complex	Temperature range (°C)	Weight loss (%)		DTG peaks (°C)	Assignments	Residue found% (calc.%)
		Obs.	Cal.			
[Cr(MFMAQ)Cl <sub>2</sub> ]	372–423	45.59	45.62	418	–C <sub>6</sub> H <sub>5</sub> NOCl <sub>2</sub>	1/2Cr <sub>2</sub> O <sub>3</sub>
	473–798	34.88	34.90	544	–C <sub>9</sub> H <sub>6</sub> NO <sub>0.5</sub>	19.71 (19.73)
[Ni(MFMAQ)Cl(H <sub>2</sub> O)]·2H <sub>2</sub> O	92–194	12.87	12.99	122, 163	–2H <sub>2</sub> O (hydrated) + H <sub>2</sub> O (coordinated)	NiO
	313–444	43.18	43.22	398	–C <sub>9</sub> H <sub>6</sub> NOCl	17.92 (17.97)
	462–799	25.72	25.77	722	–C <sub>6</sub> H <sub>5</sub> NO	
[Cu(MFMAQ)Cl(H <sub>2</sub> O)]	192–273	4.62	4.68	249	–H <sub>2</sub> O (coordinated)	CuO
	293–484	46.95	46.99	326	–C <sub>9</sub> H <sub>7</sub> NOCl	20.63 (20.68)
	506–798	27.58	27.61	565	–C <sub>6</sub> H <sub>4</sub> NO	

complexes were showed in Figures 9(a)–9(c), respectively. The micrograph of [Cr(MFMAQ)Cl<sub>2</sub>] complex shows peel shaped particles. The [Ni(MFMAQ)Cl(H<sub>2</sub>O)]·2H<sub>2</sub>O complex mentions ice rock structure. The [Cu(DPPMHQ)Cl(H<sub>2</sub>O)] complex grain-structure of ice was existent. The chemical composition of Schiff base complexes was determined using energy dispersive X-ray diffraction (EDX). In EDX profile of Cr(III), Ni(II), and Cu(II) complexes (Figures 9(a)–9(c)) the peaks of essential elements like C, N, O and respective Cr(III), Ni(II), and Cu(II) elements which constitute the molecules of [Cr(MFMAQ)Cl<sub>2</sub>], [Ni(MFMAQ)Cl(H<sub>2</sub>O)]·2H<sub>2</sub>O, and [Cu(MFMAQ)Cl(H<sub>2</sub>O)] complexes are clearly identified supporting the proposed structures. All positions contain predictable elements, and different elements such as impurity were not detected.

Figures 10(a)–10(c) show the TEM images of [Cr(MFMAQ)Cl<sub>2</sub>], [Ni(MFMAQ)Cl(H<sub>2</sub>O)]·2H<sub>2</sub>O, and [Cu(MFMAQ)Cl(H<sub>2</sub>O)] complexes, respectively. The consistency and resemblance in between the particle forms of synthesized dimeric complexes suggest that structural phases have a similar template. The particles diameter is found in nano range as follows: Cr(II), 62–224 nm; Ni(II), 18–23 nm; Cu(II), 12–32 nm. Nanoparticle-size complexes may act strong in different application areas in a biological one.

**3.2.7. Thermal Decomposition.** To evaluate the thermal behavior of metal complexes, the thermogravimetric (TG/DTG) curves for the complexes are represented in Figure 11 and weight loss at different decomposition stages, temperatures ranges with DTG peaks, assignments, and the final pyrolysis product observed in the present studies are summarized in Table 7.

In TGA curve of the [Cr(MFMAQ)Cl<sub>2</sub>] complex does not show any weight loss up to 385°C; this indicates the absence of lattice and coordinated water molecules in it. The [Cr(MFMAQ)Cl<sub>2</sub>] complex shows two-step decomposition process in the range of 372–423°C and 473–798°C, respectively; the first step is relatively fast and a total of 26.84% weight loss has been observed which corresponds to the nonchelated part of the ligand moiety. The remaining chelated part of the ligand is decomposed in the second step

which is 39.64% (calc. 38.46%). The final pyrolysis product, projected as chromium(III) oxide, and some unreacted residue had an observed mass of 33.52% (calc. 33.34%).

The TG curve of the [Ni(MFMAQ)Cl(H<sub>2</sub>O)]·2H<sub>2</sub>O complex shows the three-step decomposition process; in the first step 4.52% (calc. 4.23%) weight loss has been observed in the range of 92–124°C, which indicates the presence of one lattice water molecule in the complex. Another 4.86% (calc. 4.23%) weight loss corresponds to one coordinated water molecule which has been observed in the range of 124–173°C. In the second step of decomposition starting from 313°C to 442°C, nonchelated part of the ligand is eliminated which has been found to be 24.82% (calc. 26.04%). In the last step starting from 462°C to the final temperature, 46.84% (calc. 46.28%) weight loss corresponds to the remaining part of the ligand which has been noticed and the ultimate pyrolysis product is obtained as nickel(II) oxide of mass 18.96% (calc. 18.03%).

Quite similar results have been recorded for [Cu(MFMAQ)Cl(H<sub>2</sub>O)] where decomposition takes place in three steps in the range of 192–273°C, 293–484°C, and 506–798°C, respectively, and copper (II) oxide; mass of 21.19% (calc. 19.78%) seems to be the final product. The only difference is that no lattice water molecule is presented in [Cu(MFMAQ)Cl(H<sub>2</sub>O)] complex. On the basis of TG analysis the increasing order of the stability of complexes is as follows: [Ni(MFMAQ)Cl(H<sub>2</sub>O)]·2H<sub>2</sub>O < [Cu(MFMAQ)Cl(H<sub>2</sub>O)] < [Cr(MFMAQ)Cl<sub>2</sub>]. Thus, the Co(II) complex shows excellent thermal stability in all the complexes when subjected to higher temperature; hence it is used in such types of applications.

**3.2.8. Structure of the Complexes.** Based on the above studies, the following structure (Scheme 6) may suggest these complexes.

**3.2.9. Cytotoxicity Studies.** The anticancer activities of the H-MFMAQ Schiff base ligand and its metal(II/III) complexes against the *human breast* (MCF-7) and *lung cancer* (A549) cell lines were screened using MTT assay. The results were analyzed by cell viability curves and expressed as IC<sub>50</sub> values. The maximal inhibition concentrations (IC<sub>50</sub>) given in Table 8 showed that the cytotoxicity efficiencies of the compounds under investigation follow the order: Cr(III)

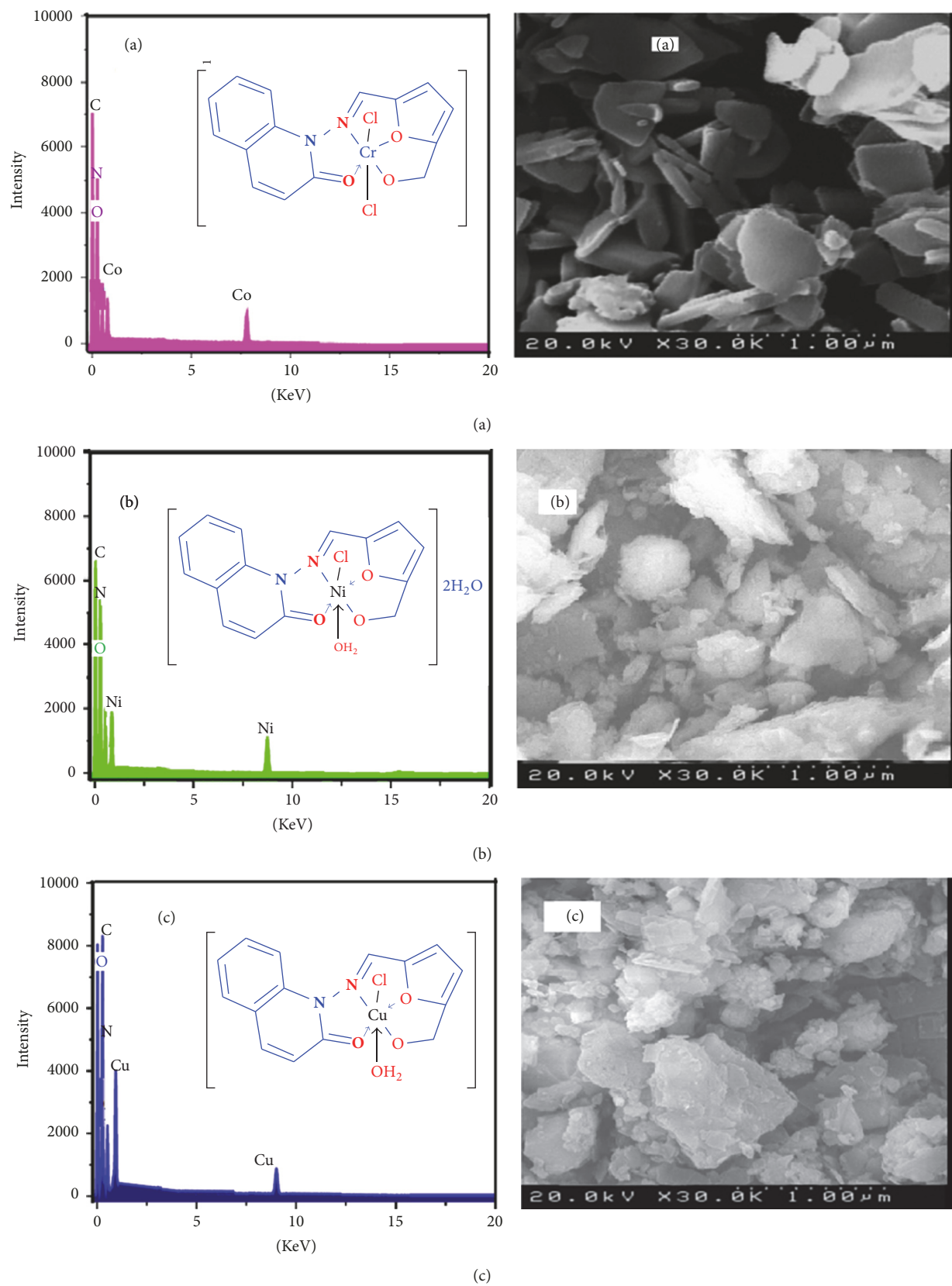


FIGURE 9: The SEM/EDX images of (a): Cr(III), (b): Ni(II), and (c): Cu(II) complexes.

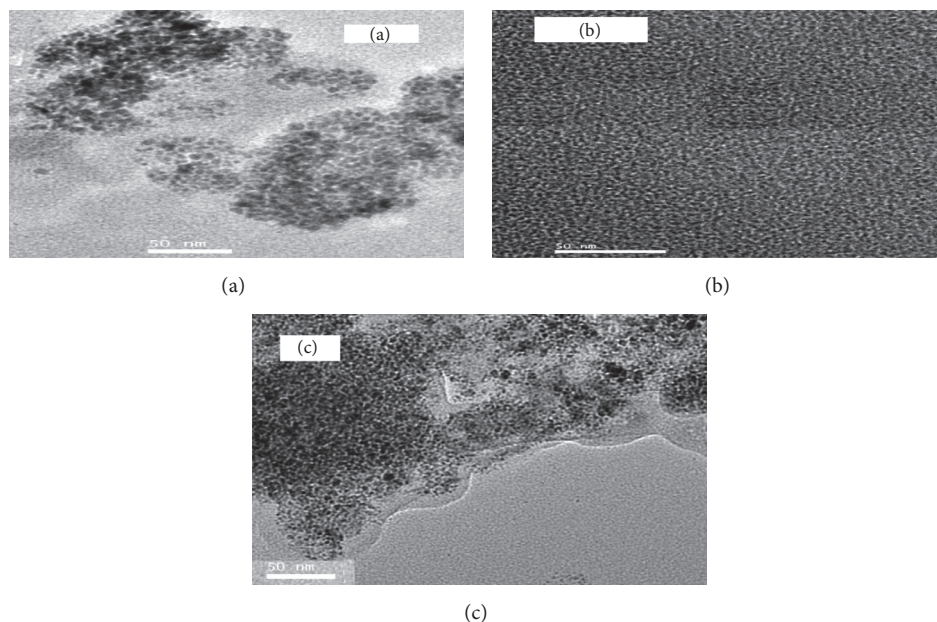


FIGURE 10: TEM images of (a): Cr(III), (b): Ni(II), and (c): Cu(II) complexes.

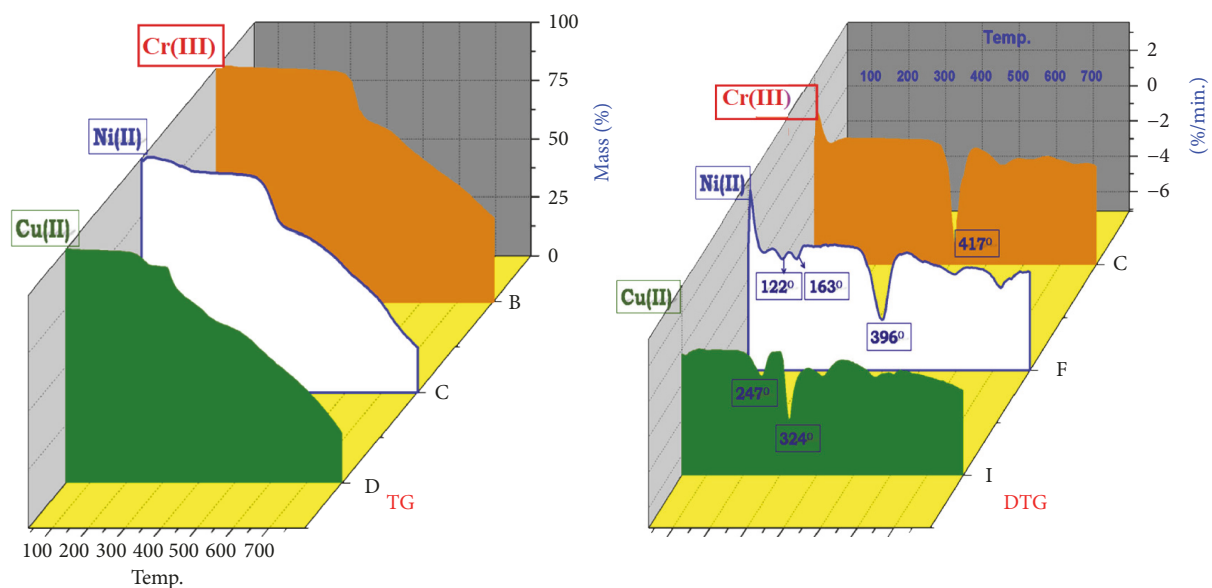


FIGURE 11: TG and DTG 3D-plots of Cr(III), Ni(II), and Cu(II) complexes up to 800°C.

complex > Ru(III) complex > H-MFMAQ > Mn(II) complex > Co(II) complex > Ni(II) complex > Cu(II) complex > Zn(II) complex. From the results, it is evident that the Cr(III) and Ru(III) complexes exhibited higher *in vitro* cytotoxicity against both the selected cell lines when compared to the Schiff base ligand. Also, the cytotoxicity efficiency of the Cr(III) and Ru(III) complexes is comparable with that of the standard drug, cis-platin, while the Mn(II), Co(II), Ni(II), Cu(II), and Zn(II) complexes showed lower anticancer activities when compared to that of the ligand. The cytotoxicity of metal complexes is depending on their ability to bind DNA

and damage its structure resulting in the impairment of its function, which is followed by replication and transcription processes inhibition and eventually cell death that is what we can suppose [22–26]. Thus, the relatively higher cytotoxicity exhibited by the Cr(III) and Ru(III) complexes may be due to the relatively stronger binding ability of the complexes with DNA as shown in the DNA binding studies.

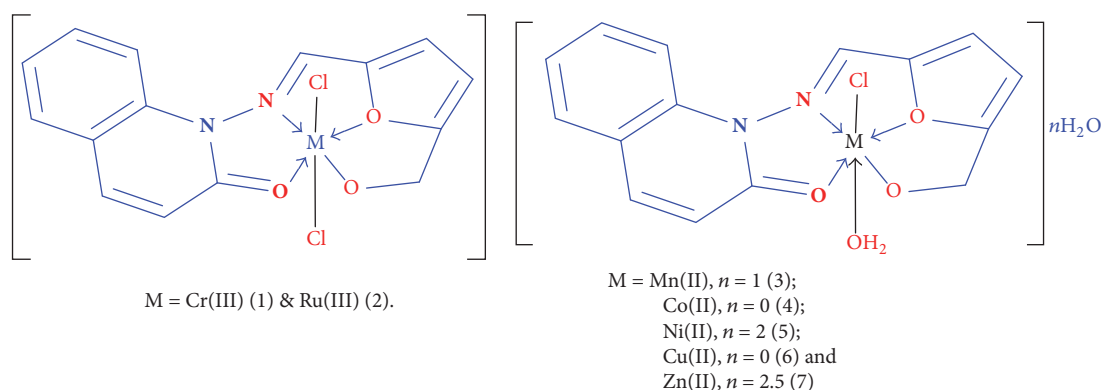
#### 4. Conclusion

The structures of the complexes of H-MFMAQ with Cr(III), Ru(III), Mn(II), Co(II), Ni(II), Cu(II), and Zn(II) ions are

TABLE 8: Cytotoxicities ( $IC_{50}$ ,  $\mu M$ ) of the Schiff base ligand and its complexes<sup>a</sup>.

Compound	MCF-7	A-549
Ligand	25 ± 1.2	28 ± 1.4
Cr(III) complex	17 ± 1.6	20 ± 1.7
Ru(III) complex	18 ± 1.5	21 ± 1.7
Mn(II) complex	21 ± 1.6	24 ± 1.6
Co(II) complex	19 ± 1.7	22 ± 1.9
Ni(II) complex	21 ± 1.7	28 ± 1.4
Cu(II) complex	26 ± 1.5	37 ± 0.8
Zn(II) complex	29 ± 1.7	38 ± 1.2
Cisplatin	13 ± 0.5	12 ± 0.9

<sup>a</sup> $IC_{50}$ : concentration of the drug required to inhibit growth of 50% of the cancer cells ( $\mu M$ ). The data are mean ± SD of three replicates each.



SCHEME 6: The proposed structures of H-MFMAQ complexes.

confirmed by the elemental analyses, IR, NMR ( $^1H$ ,  $^{13}C$ , and  $^{15}N$ ) NMR, molar conductance, magnetic moment, UV-Vis., mass, ESR, SEM, EDX, TEM, and thermal analyses data. Therefore, from the IR spectra, it is concluded that H-MFMAQ behaves as a Schiff's base tetradentate ligand with  $O_3N$  sites coordinating to the metal ions via the azomethine N group, furan O ring, carbonyl O group, and deprotonated hydroxyl-O group. From the molar conductance data of the complexes ( $\Lambda_m$ ), it is concluded that the complexes of H-MFMAQ ligand are considered as nonelectrolytes. Octahedral geometry was proposed to the Cr(III), Ru(III), Mn(II), Co(II), Ni(II), Cu(II), and Zn(II) complexes. The  $^1H$  NMR spectra of the free ligand show that the  $-OH$  signal which appeared in the spectrum of H-MFMAQ ligand at 11.35 ppm completely disappeared in the spectra of its Zn(II) complex indicating that the  $-OH$  proton is removed by the chelation with Zn(II) ion. The antitumor activities of all inspected compounds were evaluated towards *human breast* (MCF-7) and *lung cancer* (A549) cell lines.

### Conflicts of Interest

The authors declare that there are no conflicts of interest regarding the publication of this paper.

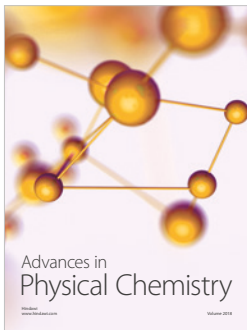
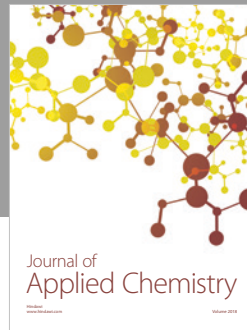
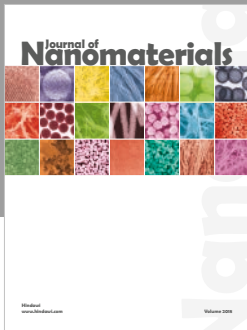
### Acknowledgments

This work was funded by the Deanship of Scientific Research at Princess Nourah Bint Abdulrahman University, through the Research Groups Program (Grant no. RGP-1438-00...).

### References

- [1] B. Zhang, S. Li, E. Herdtweck, and F. E. Kühn, "Schiff base complexes of methyltrioxorhenium (VII): Synthesis and catalytic application," *Journal of Organometallic Chemistry*, vol. 739, pp. 63–68, 2013.
- [2] M. K. Taylor, J. Reglinski, and D. Wallace, "Coordination geometry of tetradentate Schiff's base nickel complexes: The effects of donors, backbone length and hydrogenation," *Polyhedron*, vol. 23, no. 18, pp. 3201–3209, 2004.
- [3] H.-C. Wu, P. Thanasekaran, C.-H. Tsai et al., "Self-assembly, reorganization, and photophysical properties of silver(I)-Schiff-base molecular rectangle and polymeric array species," *Inorganic Chemistry*, vol. 45, no. 1, pp. 295–303, 2006.
- [4] E. Kwiatkowski, G. Romanowski, W. Nowicki, M. Kwiatkowski, and K. Suwińska, "Chiral dioxovanadium(V) complexes with single condensation products of 1,2-diaminocyclohexane and aromatic o-hydroxycarbonyl compounds: synthesis, characterization, catalytic properties and structure," *Polyhedron*, vol. 26, no. 12, pp. 2559–2568, 2007.

- [5] N. K. Chaudhary and P. Mishra, "Metal complexes of a novel schiff base based on penicillin: characterization, molecular modeling, and antibacterial activity study," *Bioinorganic Chemistry and Applications*, vol. 2017, Article ID 6927675, 13 pages, 2017.
- [6] N. A. Negm, M. F. Zaki, and M. A. I. Salem, "Cationic schiff base amphiphiles and their metal complexes: Surface and biocidal activities against bacteria and fungi," *Colloids and Surfaces B: Biointerfaces*, vol. 77, no. 1, pp. 96–103, 2010.
- [7] T. Arun, R. Subramanian, and N. Raman, "Novel bio-essential metal based complexes linked by heterocyclic ligand: Synthesis, structural elucidation, biological investigation and docking analysis," *Journal of Photochemistry and Photobiology B: Biology*, vol. 154, pp. 67–76, 2016.
- [8] A. Y. Lukmantara, D. S. Kalinowski, N. Kumar, and D. R. Richardson, "Synthesis and biological evaluation of 2-benzoylpyridine thiosemicarbazones in a dimeric system: Structure-activity relationship studies on their anti-proliferative and iron chelation efficacy," *Journal of Inorganic Biochemistry*, vol. 141, no. 1, pp. 43–54, 2014.
- [9] J. Hung and L. M. Werbel, "Investigations into the synthesis of 6-ethyl-5-(4-pyridinyl)-2,4-pyrimidinediamine as a potential antimalarial agent," *Journal of Heterocyclic Chemistry*, vol. 21, no. 3, pp. 741–744, 1984.
- [10] M.-H. Wu and W.-D. Zou, "Electronic structure of the organic half-metallic magnet: 2-(5-pyrimidinyl)-4,4,5,5-tetramethyl-4,5-dihydro-1 H-3-oxoimidazol-1-oxyl," *Journal of Mathematical Chemistry*, vol. 40, no. 3, pp. 319–325, 2006.
- [11] H. Bayrak, A. Demirbas, S. A. Karaoglu, and N. Demirbas, "Synthesis of some new 1,2,4-triazoles, their Mannich and Schiff bases and evaluation of their antimicrobial activities," *European Journal of Medicinal Chemistry*, vol. 44, no. 3, pp. 1057–1066, 2009.
- [12] W. J. Geary, "The use of conductivity measurements in organic solvents for the characterisation of coordination compounds," *Coordination Chemistry Reviews*, vol. 7, no. 1, pp. 81–122, 1971.
- [13] R. F. M. Elshaarawy, Z. H. Kheiralla, A. A. Rushdy, and C. Janiak, "New water soluble bis-imidazolium salts with a saldach scaffold: Synthesis, characterization and in vitro cytotoxicity/bactericidal studies," *Inorganica Chimica Acta*, vol. 421, pp. 110–122, 2014.
- [14] J. A. Faniran, K. S. Patel, and L. O. Nelson, "Physico-chemical studies of metal  $\beta$ -diketonates-I Infrared spectra of 1-(3-pyridyl)-1,3-butanedione and its divalent metal complexes," *Journal of Inorganic and Nuclear Chemistry*, vol. 38, no. 1, pp. 77–80, 1976.
- [15] N. Raman, J. Dhavethu Raja, and A. Sakthivel, "Template synthesis of novel 14-membered tetraazamacrocyclic transition metal complexes: DNA cleavage and antimicrobial studies," *Journal of the Chilean Chemical Society*, vol. 53, no. 3, pp. 1568–1571, 2008.
- [16] A. Kumar, A. K. Jha, N. Mazumdar, S. N. Yadav, and L. K. Mishra, "Complexes of Nickel-, Zinc-, Palladium- And Cadmium(II) with some Furan-2-thiohydrazones," *Journal of the Indian Dental Association*, vol. 74, no. 6, pp. 485–486, 1997.
- [17] K. Nakamoto, *Infrared and Raman Spectra of Inorganic and Coordination Compounds*, John Wiley & Sons, Inc, NY, USA, 2009.
- [18] J. Owen, "The magnetic evidence for charge transfer in octahedral complexes," *Discussions of the Faraday Society*, vol. 19, pp. 127–134, 1955.
- [19] H. Montgomery and E. C. Lingafelter, "The crystal structure of Tutton's salts. IV. Cadmium ammonium sulfate hexahydrate," *Acta Crystallographica*, vol. 20, no. 6, pp. 728–730, 1966.
- [20] R. Shirley, *The crysfire system for automatic powder indexing: users manual*, The Lattice Press, Guildford Park Avenue, Guildford, Surrey GU2 7NL, England, UK, 2000.
- [21] A.-N. M. A. Alaghaz, M. E. Zayed, S. A. Alharbi, R. A. A. Ammar, and A. Chinnathambi, "Synthesis, spectroscopic identification, thermal, potentiometric and antibacterial activity studies of 4-amino-5-mercapto-S-triazole Schiff's base complexes," *Journal of Molecular Structure*, vol. 1087, pp. 60–67, 2015.
- [22] F. Denizot and R. Lang, "Rapid colorimetric assay for cell growth and survival—modifications to the tetrazolium dye procedure giving improved sensitivity and reliability," *Journal of Immunological Methods*, vol. 89, no. 2, pp. 271–277, 1986.
- [23] T. Mosmann, "Rapid colorimetric assay for cellular growth and survival: application to proliferation and cytotoxicity assays," *Journal of Immunological Methods*, vol. 65, no. 1-2, pp. 55–63, 1983.
- [24] E. Gao, Y. Sun, Q. Liu, and L. Duan, "An anticancer metal-lobenzylmalonate: Crystal structure and anticancer activity of a palladium complex of 2,2'-bipyridine and benzylmalonate," *Journal of Coordination Chemistry*, vol. 59, no. 11, pp. 1295–1300, 2006.
- [25] M. Ferrari, M. C. Fornasiero, and A. M. Isetta, "MTT colorimetric assay for testing macrophage cytotoxic activity in vitro," *Journal of Immunological Methods*, vol. 131, no. 2, pp. 165–172, 1990.
- [26] N. A. Rey, A. Neves, P. P. Silva et al., "A synthetic dinuclear copper(II) hydrolase and its potential as antitumoral: Cytotoxicity, cellular uptake, and DNA cleavage," *Journal of Inorganic Biochemistry*, vol. 103, no. 10, pp. 1323–1330, 2009.



Hindawi

Submit your manuscripts at  
[www.hindawi.com](http://www.hindawi.com)

